Journal of CO2 Utilization 72 (2023) 102508

Contents lists available at ScienceDirect

Journal of CO2 Utilization

journal homepage: www.elsevier.com/locate/jcou

Evaluation of CO_2 sources for Power-to-Liquid plants producing Fischer-Tropsch products

Simon Pratschner [*,1], Martin Hammerschmid [2], Stefan Müller [3], Franz Winter [4]

Technische Universität Wien, Faculty of Technical Chemistry, Institute of Chemical, Environmental and Bioscience Engineering, Getreidemarkt 9/166, 1060 Vienna, Austria

ARTICLE INFO

Keywords:
Power-to-Liquid
Carbon capture and utilization
Solid-oxide electrolysis
Fischer-Tropsch synthesis
Process simulation
CO_2 sources

ABSTRACT

In addition to the climate crisis's looming dangers, Europe was recently affected by profoundly volatile energy markets, entailing soaring inflation and political uncertainty. Power-to-Liquid processes have the potential to curb global warming by valorizing CO_2 to produce synthetic fuels and platform chemicals while simultaneously substituting fossil energy imports. The impact of the CO_2 source, i.e., cement production, biogas upgrading and solid biomass combustion, on Power-to-Liquid plants was evaluated by implementing the designed configuration, including CO_2 capture, solid-oxide electrolyzer, Fischer-Tropsch synthesis and steam reforming, in IPSEpro, a stationary equation-based process simulation tool. Maximum Power-to-Liquid efficiency of 63.8% and maximum carbon efficiency of 88.6% were obtained by exploiting CO_2 emitted by a biogas upgrading unit. Solid-oxide electrolyzers ranging from 23 $MW_{el.}$ (biogas) to 504 $MW_{el.}$ (cement) are required to process CO_2 streams from 4.5 to 100 t/h. In addition, the mass and energy balances of the three considered configurations were determined and embedded in a process flow diagram. The presented study aims to facilitate future decisions concerning carbon capture and utilization policy by assessing the CO_2 source's influence on Power-to-Liquid plants' key performance indicators. Furthermore, the underlying work supports a sustainable realization of Power-to-Liquid plants by offering a framework for exploiting CO_2 sources.

1. Introduction

The climate crisis poses a major threat to global peace and prosperity in the upcoming decades. A global mean level of 414.6 ppm CO_2 was reported by the National Oceanic and Atmospheric Administration in September 2022, an increase of 2.6 ppm compared to September 2021 [49]. Responsible for this worrying increase are global CO_2 emissions of around 36 Gt per year, of which 2.4 Gt are directly emitted by the European Union's 27 member states [31]. The transport sector can be seen as the EU27's weak spot, which in contrast to all other sectors, still rises annually [8]. The respective CO_2 emissions can be allocated to road transportation (20.5%), marine navigation (4.0%) and aviation (3.8%) [18]. To combat this unsatisfactory development, the European Parliament has recently backed the European Commission's proposal of banning CO_2 emissions caused by private transport as of 2035. However, the opaque wording still leaves scope for interpretation and thus, sustainable synthetic fuels are still in the race to compete with individual electric mobility. In addition, hard-to-abate sectors, i.e., aviation, marine navigation and heavy-duty applications, still rely on high energy density fuels. Due to the vehicles' high mass, substituting conventional fuels with electricity or H_2 remains disadvantageous. Millinger et al. provide a comprehensive overview of the EU's transport sector and its projected development until 2050 [47]. The total transport fuel demand

Abbreviations: ASF, Anderson-Schulz-Flory distribution; BECCU, bioenergy with carbon capture and utilization; CCU, carbon capture and utilization; CHP, combined heat and power; DC, direct current; eASF, extended Anderson-Schulz-Flory distribution; El, electric; EU, European Union; FT, Fischer-Tropsch; KPI, key performance indicator; M, electric motor; MEA, monoethanolamine; No., stream number; P, pump; PtL, Power-to-Liquid; PtX, Power-to-X; Ref., Reformer; rWGS, reverse water-gas shift; SBCR, slurry bubble column reactor; SOEC, solid-oxide electrolysis cell; SOEL, solid-oxide electrolyzer; Sol., solution; SR, steam reformer; TG, tail gas; V, blower, compressor; W, heat exchanger.

* Corresponding author.
E-mail address: simon.pratschner@tuwien.ac.at (S. Pratschner).
[1] 0000-0001-6167-586X
[2] 0000-0002-1155-926X
[3] 0000-0001-8878-429X
[4] 0000-0001-9854-3836

https://doi.org/10.1016/j.jcou.2023.102508
Received 3 March 2023; Received in revised form 23 May 2023; Accepted 23 May 2023

Nomenclature

Parameters

$E_{Chem.}$	chemical energy MW_{ch}
H_2:CO	H_2 to CO ratio
m	mass flow rate kg/s, t/h
M	molar mass kg/kmol
n	molar flow rate kmol/h
P	power MW_{el}
p	pressure Pa, bar
RR	recirculation ratio %
RU	reactant utilization -, %
T	temperature °C, K
w	mass fraction wt%
X	conversion -, %
y	volume fraction vol%
ΔG_r	free Gibbs energy kJ/mol
ΔH_r	reaction enthalpy kJ/mol
ΔS_r	reaction entropy kJ/(mol•K)
η_{Carbon}	carbon efficiency %
η_{PtL}	Power-to-Liquid efficiency %
ρ	density kg/m^3

Table 1
Ongoing and planned Power-to-Liquid projects in Europe.

Company/ Project	Site	Year	Technology	Output	Source
Ineratec	Hamburg, GER	2022	FT	350 t/a	[35]
Ineratec	Frankfurt, GER	2024	FT	2500 t/a	[24]
ICO2CHEM	Frankfurt, GER	Ongoing	FT	-	[30]
Norsk e-fuel	Mosjøen, NOR	2024	FT	12.5 ML/a	[51]
Norsk e-fuel	Mosjøen, NOR	2026	FT	25 ML/a	[51]
Norsk e-fuel	Mosjøen, NOR	2029	FT	100 ML/a	[51]
Nordic Electrofuel	Porsgrunn, NOR	2025	FT	10 ML/a	[50]
Nordic Electrofuel	Porsgrunn, NOR	-	FT	200 ML/a	[50]
C2PAT	Mannersdorf, AUT	Ongoing	FT	2500 t/a[1])	[44]
Carbon2Chem	Duisburg, GER	Ongoing	Methanol, NH_3	-	[70]
Lipor	Porto, POR	tba	-	-	[40]

1) Calculation based on a stated CO_2 input of 10,000 t/a.

was 4851 TWh in 2018 and is anticipated to rise constantly within the following decades. The increase of aviation passenger kilometers is predicted to increase by 50% until 2040 and 100% until 2060. The demand for maritime fuel will increase by 50% until 2050.

Power-to-Gas (PtG) applications, i.e., H_2 and methane, have dominated Power-to-X (PtX) projects in Europe in the past years with a share of around 90% [75]. However, the pressing demand for sustainable solutions for the maritime and aviation industry has sparked an increased interest in Power-to-Liquid (PtL) plants, producing either methanol or fuels derived from Fischer-Tropsch (FT) products. An excerpt of ongoing PtL projects is given by Pratschner et al. [57]. Recently announced PtL projects are listed in Table 1. In addition, Ineratec has declared an upcoming cooperation with Japanese and Asian-pacific partners to establish industrial PtL plants in East and South East Asia [34].

The utilized CO_2 source is a critical factor when assessing the sustainability of PtL processes. The following properties need to be considered to maximize the PtL plant's potential to curb the climate crisis:

- Origin of CO_2, i.e., biogenic, inorganic or fossil CO_2.
- The concentration of CO_2, e.g., point sources vs. direct air capture.
- Amount of CO_2, i.e., the mass flow rate of point sources.

The concentration of CO_2 sources can vary from 400 ppm (direct air capture) to up to 98 vol% (biogas upgrading plant). Thermodynamically, the required energy, i.e., heat and electricity, to capture and separate CO_2 from air, industrial streams or power plants mainly depends on the CO_2 source's concentration. CO_2 capture technologies must be designed specifically to the gas stream's conditions, e.g., concentration, temperature and pressure. Vaz et al. provide an extensive overview of state-of-the-art CO_2 capture technologies [71]. Combined heat and power (CHP) plants emit an off-gas with a share of about 10–15 vol% CO_2. Likewise, the mass flow rates of typical CO_2 sources underlie vast differences ranging from around 120 t per day for a decentralized biomass heating plant and 103,000 t per day for Europe's largest coal plant in Belchatów, Poland [48].

Capturing CO_2 entails a high demand for thermal energy. Identifying and exploiting industrial waste heat streams thus have the potential to facilitate Power-to-Liquid plants. Bianchi et al. estimate the feasible potential of waste heat in the EU at 279 TWh/a. High-temperature waste heat streams surpassing temperatures of 300 °C hold a share of 55% of the stated potential [4]. Energy-intensive processes, e.g., steam generation and CO_2 desorption, could be supplied by enforcing sector coupling. An extensive review of conventional waste heat recovery technologies is provided by Jouhara et al. [36].

A cement plant, a biogas upgrading plant and a biomass CHP plant were elected as CO_2 sources within the presented study. Cement and clinker production has been studied in detail in numerous studies [29,5,74,10]. The cement industry is a major emitter of CO_2, responsible for 7% [33] of the global and 3% of the EU's CO_2 emissions [14]. Biogas upgrading plants provide a highly concentrated biogenic CO_2 stream and, thus, are predestined to serve as CO_2 sources for PtL applications. Operators of biogas upgrading plants must comply with local feed-in standards. Therefore, separating CO_2 from the main product CH_4 is a legal requirement. Downstream PtL plants are a viable solution to upgrade the by-product CO_2 to higher-grade products. As calculated by Millinger et al. [47], the biogas potential in Europe lies between 3.2% and 9.0% of the EU27's primary energy demand [17]. State-of-the-art biogas plants are a promising solution to increase the share of sustainable fuels and thus have received increased interest in recent studies [15,19,55,65,9]. Using solid biomass as an energy source underlies a controversial discussion in the EU27. According to the projections by Millinger et al., 2.5–14.9% of the EU27's primary energy demand can be covered by the combustion of solid biomass within the upcoming decades [16,47].

This study's main objective is to determine the CO_2 source's influence on the performance of PtL plants. In addition, a recommendation on which CO_2 sources should be prioritized to maximize PtL plants' potential to curb the environmental crisis will be given. The following research questions are posed to achieve the stated goals:

1. Which CO_2 sources should be prioritized for carbon capture and utilization applications based on Power-to-Liquid processes combining solid-oxide electrolysis and Fischer-Tropsch synthesis?
2. Which effect does the CO_2 source have on the key performance indicators of Power-to-Liquid plants?

Table 2
Chosen CO_2 sources for the presented case studies of Power-to-Liquid plants.

Sources for CO_2 feed streams			[7,6]	[15]	[56]
Parameter	Symbol	Unit	Cement plant[1)]	Biogas upgrading[2)]	CHP[3)]
Mass flow of CO_2	$\dot{m}_{CO_2}$	kg/h	100,000	4600	7700
Volume share CO_2	y_{CO_2}	vol %	19.0	98.0	14.3
Volume share N_2	y_{N_2}	vol %	61.0	-	82.3
Volume share H_2O	y_{H_2O}	vol %	10.0	0.3	0.4
Volume share CH_4	y_{CH_4}	vol %	-	1.7	-
Volume share O_2	y_{O_2}	vol %	10.0	-	3.0

1) Annual cement production of 1.2 million tons
2) Annual production of 30.5 million Nm^3 CH_4 (corresponds to 38 MW)
3) Thermal power input of 20 $MW_{th.}$. The flue gas is cooled to a temperature of 15 °C.

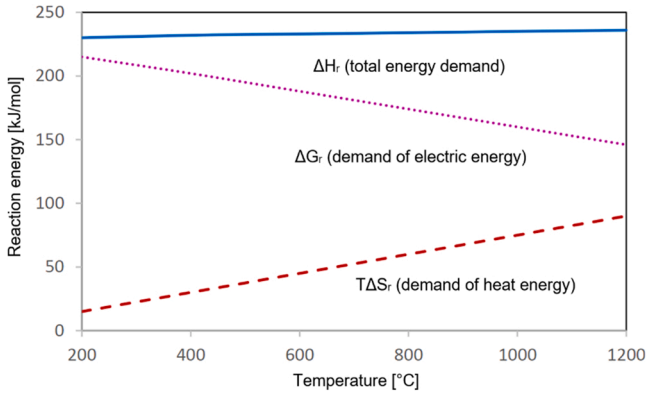

Fig. 1. Allocation of high-temperature electrolyzers' energy demand as a function of the temperature.
Reprinted with permission from [2] . Copyright 2020 Elsevier.

2. Methodology

The underlying study is founded on the obtained mass and energy balances of a Power-to-Liquid plant by applying IPSEpro 8.0, a stationary equation-based process simulation tool. The presented plant configuration is based on previous modeling work concerning the Fischer-Tropsch synthesis [57]. In addition, the following subprocesses were modeled and added to the existing process simulation flowchart:

- CO_2 capture by a monoethanolamine (MEA) absorption process.
- Solid-oxide electrolyzer (SOEL) operating in co-electrolysis mode.
- Steam reformer for tail gas reforming.

The subprocess modeling is elaborated on in further detail. Furthermore, the PtL plant's chosen key performance indicators (KPI) are defined to facilitate the comparison between the three analyzed CO_2 sources, i.e., a cement plant, a biogas upgrading plant and a CHP plant burning wood chips.

2.1. CO_2 sources

Three different CO_2 sources were taken as a foundation for the simulated PtL plant:

1. Norcem Brevik cement plant in Porsgrunn, Norway [7].
2. Biogas upgrading plant in Montello, Italy [15].
3. Decentralized CHP plant burning wood chips [56].

Table 2 displays the CO_2 sources' features.

2.2. Key performance indicators

The following KPIs were defined to facilitate the comparability between the presented scenarios.

2.2.1. Carbon efficiency η_{Carbon}

The carbon efficiency is defined as the ratio of carbon atoms being transformed into Fischer-Tropsch products, i.e., naphtha, middle distillate and wax, and calculated according to Eq. 1. Carbon atoms are inserted into the PtL plant as CO_2 or CH_4 molecules within the feed gas stream and emitted as CO_2 after the purge gas combustion.

$$\eta_{Carbon} = \frac{\dot{n}_{Carbon,in} - \dot{n}_{Carbon,out}}{\dot{n}_{Carbon,in}} \quad (1)$$

2.2.2. Power-to-Liquid efficiency η_{PtL}

The Power-to-Liquid efficiency η_{PtL} is defined as the ratio of chemically stored energy in the Fischer-Tropsch products and the PtL plant's total electricity demand, i.e., to power the SOEL unit, the syngas compressor, pumps and other auxiliary equipment.

$$\eta_{PtL} = \frac{E_{Chem.,FT\ products}}{P_{in,\ Total}} \quad (2)$$

2.2.3. Conversion of carbon monoxide X_{CO} and recirculation ratio of tail gas RR

The conversion of carbon monoxide is distinguished between the Fischer-Tropsch reactor's per pass CO conversion $X_{CO,FT}$ and the CO conversion at system level $X_{CO,System}$, see Eq. 3. Besides the per pass conversion, the recirculation ratio of tail gas RR, see Eq. 4, is a decisive factor influencing the system's total CO conversion.

$$X_{CO} = \frac{\dot{n}_{CO,in} - \dot{n}_{CO,out}}{\dot{n}_{CO,in}} \quad (3)$$

$$RR = \frac{\dot{m}_{Recirculated\ tail\ gas}}{\dot{m}_{Total\ tail\ gas}} \bullet 100\% \quad (4)$$

2.2.4. Scale of the solid-oxide electrolyzer P_{SOEL}

The electrolyzer's scale in $MW_{el.}$ is a benchmark parameter for the respective Power-to-Liquid plant size. In addition, P_{SOEL} can be used to ensure comparability to other conventional, e.g., fossil refineries, and innovative processes, e.g., Biomass-to-Liquid.

2.3. Fischer-Tropsch synthesis

A detailed elaboration of the Fischer-Tropsch process modeling has been conducted in a previous study [57]. The underlying model is based on assumptions concerning a low-temperature Fischer-Tropsch process, operating at a temperature of $T_{FT} = 230$ °C and a pressure of $p_{FT} = 21$ bar, realized in a slurry bubble column reactor (SBCR). A per-pass CO conversion of $X_{CO,FT} = 55\%$ was assumed. The synthesized Fischer-Tropsch products are considered paraffinic only, as shown by Eq. 5.

$$n\ CO + (2n+1)\ H_2 \rightarrow H(CH_2)_n H + n\ H_2O, \qquad \Delta H_R = -166.4 kJ/mol \quad (5)$$

The extended Anderson-Schulz-Flory (eASF) distribution, as established by Förtsch et al., has been applied to compensate for the standard ASF distribution's weaknesses, i.e., underestimation of CH_4 forming, overestimation of C_2H_6 and a lack of differentiation between short- and long-chained hydrocarbons [20]. The applied parameters and

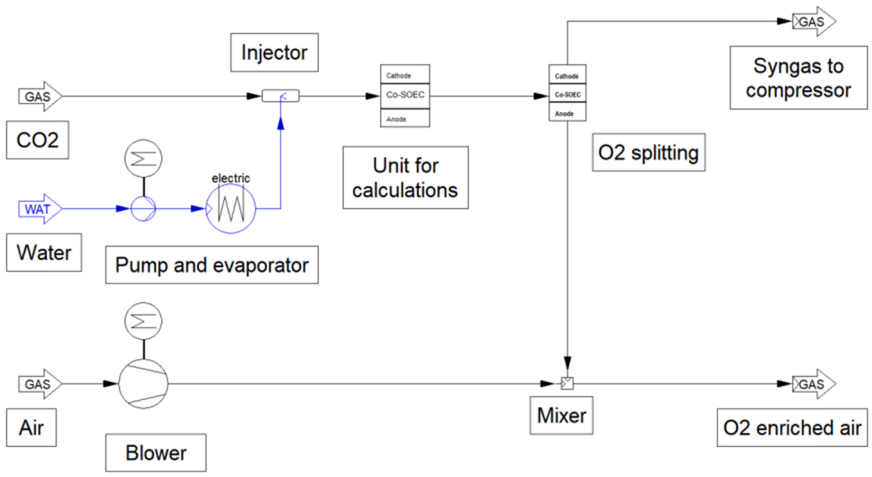

Fig. 2. Modeling of the solid-oxide electrolyzer in co-electrolysis mode.

assumptions concerning the eASF distribution are based on a previously conducted study [57].

A substantial technological effort is required to process Fischer-Tropsch syncrude into jet fuel, complying with international standards. Downstream processes such as hydrocracking, dehydrogenation, oligomerization and aromatization are necessary to adjust the hydrocarbon chain length and structure. A detailed elaboration of a Fischer-Tropsch syncrude refinery is given by Petersen et al., [54], suggesting a combined refinery efficiency of 86% with an additional H_2 demand of 0.016 kg H_2/kg fuel.

2.4. Solid-oxide electrolyzer in co-electrolysis mode

Solid-oxide electrolyzers exploit the decreasing demand for electric energy at increasing temperatures, concluding in a smaller power demand than low-temperature electrolysis technologies, i.e., alkaline water electrolysis and proton exchange membrane electrolysis. Fig. 1 displays the thermodynamic principle. The total energy required for water splitting (ΔH_r) is the sum of provided electric energy (ΔG_r) and heat energy ($T\Delta S_r$). Thus, the electrolyzer's power demand decreases with increasing temperatures.

State-of-the-art SOEL units operate at temperatures ranging from 800° to 900°C and at a pressure slightly above ambient pressure levels [62]. The world's first multi-megawatt high-temperature electrolyzer was installed in Rotterdam, the Netherlands, in April 2023, with a rated power of 2.6 $MW_{el.}$ [67]. Typical SOEL catalyst systems are based on dispersed nickel in an yttria-stabilized zirconia framework. Thus, a catalyst guard system is recommended to avoid catalyst poisoning [64]. In co-electrolysis mode, H_2O and CO_2 are converted to syngas. The chemical reactions occurring at the cathode under the provision of electrons are shown by Eq. 6 and 7.

$$H_2O\ (g) + 2\ e^- \rightarrow O^{2-} + H_2\ (g) \tag{6}$$

$$CO_2\ (g) + 2\ e^- \rightarrow O^{2-} + CO\ (g) \tag{7}$$

The generated oxygen ions are transferred to the anode via the solid electrolyte, where they are subsequently oxidized to gaseous O_2, as shown in Eq. 8.

$$2\ O^{2-} \rightarrow O_2\ (g) + 4\ e^- \tag{8}$$

Due to the increased operating temperatures of 800–900 °C, the rWGS reaction occurs, shown by Eq. 9.

$$CO_2 + H_2 \rightarrow CO + H_2O, \quad \Delta H_r = 41.2 kJ/mol \tag{9}$$

Wang et al. stated that almost no direct splitting of CO_2 occurred within their experimental tests and that the rWGS reaction is the main driver for the conversion of CO_2 to CO [72]. Thus, Eq. 7 is neglected for the presented SOEL model. Additional H_2 needs to be provided by the electrolyzer to meet the rWGS reaction's demand.

According to Cinti et al., the cell operating conditions have only a minor influence on the H_2:CO ratio provided by the SOEL unit [11]. It is instead determined by the feed ratio of H_2O to CO_2. The H_2:CO ratio of the syngas leaving the electrolyzer can be set within the presented model. The feed mass flow rates of H_2O and CO_2 are automatically adjusted to meet the required specifications. The conversion of H_2O and CO_2 is defined by Eq. 10 and Eq. 11. In addition, the reactant utilization RU is defined as the total conversion of feed streams, as seen in Eq. 12.

$$X_{H_2O} = \frac{\dot{n}_{H_2O,in} - \dot{n}_{H_2O,out}}{\dot{n}_{H_2O,in}} \tag{10}$$

$$X_{CO_2} = \frac{\dot{n}_{CO_2,in} - \dot{n}_{CO_2,out}}{\dot{n}_{CO_2,in}} \tag{11}$$

$$\mathrm{RU} = \frac{(\dot{n}_{CO_2,in} + \dot{n}_{H_2O,in}) - (\dot{n}_{CO_2,out} + \dot{n}_{H_2O,out})}{(\dot{n}_{CO_2,in} + \dot{n}_{H_2O,in})} \tag{12}$$

The electrolyzer's power demand is determined by the volume flow rate of H_2 leaving the SOEL unit and the required H_2 for converting CO_2 to CO via the rWGS reaction. Schmidt et al. propose a specific power demand of 3.2 (at stack level) to 3.7 (at system level) $kWh_{el.}/Nm^3$ H_2 [62]. Other sources list values ranging from 3.2 to 3.6 $kWh_{el.}/Nm^3$ H_2 [21,59,68]. A specific power demand of 3.37 $kWh_{el.}/Nm^3$ H_2 was chosen within this study according to the HELMETH project's outcome [26].

A detailed overview of the SOEL modeling can be found in Fig. 2. Steam and CO_2 are mixed before entering the main unit, where all stoichiometric and energy calculations occur. A subsequent unit separates the generated O_2 from the syngas stream. The removal of O_2 molecules from the anodic layer must be ensured in real applications to avoid mass transfer limitations. Thus, the separated O_2 leaving the SOEL's anode, is mixed with ambient air at an air:O_2 ratio of 1. The generated syngas leaves the electrolyzer at the cathodic side and gets transferred to the subsequent syngas condenser and compressor.

Numerous studies have focused on state-of-the-art solid-oxide electrolyzers, including applied materials [27,37,42,62,72]. Modeling SOEL units has been a major objective of various research articles [2,12,11,42,45,72,76]. In addition, several experimental studies have been conducted to evaluate established models of solid-oxide electrolyzers [11,25,66,76].

2.5. CO_2 capture – MEA absorption

CO_2 capture by MEA absorption is a mature technology. An MEA

Table 3
List of considered heat sources and sinks.

Heat sources				Heat sinks			
Unit	Material	T_{in} [°C]	T_{out} [°C]	Unit	Material	T_{in} [°C]	T_{out} [°C]
TG	Flue gas	1100	50	CO_2 capture	MEA[2)]	120	120
FT	Steam[1)]	220	220	CO_2 capture	H_2O	20	120
W8	Tail gas	850	50	SOEL	H_2O	20	200
W1	Syngas	850	20	Reformer	H_2O	20	200
				SOEL $\Delta H_r^{3)}$	-	850	850
				Ref. $\Delta H_r^{3)}$	-	850	850
				W7	Tail gas	30	850
				SOEL	CO_2, H_2O	120	850

1) Boiling water reactor - evaporation of boiling water
2) Heat demand of CO_2 desorption
3) Reaction enthalpy of occurring chemical reactions.

solution circulates between an absorber column, usually operating at temperatures of around 35 °C [39], and a desorber column, operating at elevated temperatures of about 120 °C [73]. Heat must be applied to regenerate the loaded solution, concluding in a specific heat demand of 3.1–4.0 $GJ_{th.}/t$ CO_2 [39,58,73]. Current state-of-the-art CO_2 capture units based on MEA absorption obtain capture efficiencies of up to 90% [5,29,58,73] with gas purities higher than 99.9 vol% [46].

According to Machida et al., the heat demand of CO_2 capture by an MEA solution can be allocated as follows [41]:

- 53% reaction heat to dissolve the bound CO_2.
- 16% sensible heat to heat the loaded solution.
- 31% latent heat to evaporate the steam for stripping.

The mass flow rate of steam should be between 50 and 77 wt% of the CO_2 mass flow rate to ensure a sufficient desorption process [41,58].

In this study, the pump's electric duty was calculated according to Eq. 14 for an assumed mass fraction of MEA of $w_{MEA} = 0.35$ kg MEA/kg solution and a CO_2 loading difference of 0.2 between the absorber and the desorber [38]. A typical density of a 40 wt% MEA solution is 1100 kg/m^3 [23]. A pressure drop of 0.3 bar was assumed for the MEA solution [52].

$$\dot{m}_{MEA} = \frac{\dot{m}_{CO_2}}{0.35 \frac{kg\ MEA}{kg\ Solution} \bullet 0.2 \bullet \frac{M_{CO_2}}{M_{MEA}}} \tag{13}$$

$$P_{Pump} = \frac{\dot{m}_{Solution}}{\rho_{Solution}} \bullet \Delta p_{MEA} \tag{14}$$

2.6. Steam reforming of recirculated tail gas

A steam reformer has been implemented to reform hydrocarbons within the recirculated tail gas stream. In addition, CO_2 is converted to CO via the rWGS reaction. A temperature level of $T_{Reformer} = 850$ °C was chosen to maximize hydrocarbon conversion into syngas and shift the rWGS reaction's thermodynamic equilibrium to the product side. From a thermodynamic perspective, the reformer's pressure level should be as low as possible. The following chemical reactions were implemented in the designed model.

$$CH_4 + H_2O \rightarrow CO + 3H_2,\ \Delta H_r = 206.1 kJ/mol \tag{15}$$

$$C_2H_6 + 2H_2O \rightarrow 2CO + 5H_2,\ \Delta H_r = 347.3 kJ/mol \tag{16}$$

$$C_3H_8 + 3H_2O \rightarrow 3CO + 7H_2,\ \Delta H_r = 497.7 kJ/mol \tag{17}$$

$$CO_2 + H_2 \rightarrow CO + H_2O,\ \Delta H_r = 41.2 kJ/mol \tag{18}$$

The conversion of hydrocarbons is based on a stoichiometric calculation according to Eq. 19. Based on the experimental investigations conducted by Schädel et al., the following conversions of hydrocarbons were assumed at a temperature of 850 °C and a pressure of 1 bar [61].

$$X_{C_xH_y} = \frac{\dot{n}_{C_xH_y,in} - \dot{n}_{C_xH_y,out}}{\dot{n}_{C_xH_y,in}} \tag{19}$$

- Conversion of methane $X_{CH4} = 90\%$.
- Conversion of ethane $X_{C2H6} = 95\%$.
- Conversion of propane $X_{C3H8} = 99\%$.

The steam to carbon ratio S/C is defined as the steam's molar flow rate divided by the carbon atoms' molar flow rate bound within the reformed hydrocarbons, see Eq. 20. S/C ratios between 2.2 and 4.0 are recommended [2,61]. A detailed explanation of the S/C ratio's effects on process performance is given by Adiya et al. [1].

$$S/C = \frac{\dot{n}_{H_2O}}{\dot{n}_{CH_4} + 2 \bullet \dot{n}_{C_2H_6} + 3 \bullet \dot{n}_{C_3H_8}} \tag{20}$$

The rWGS reaction's activity inside the steam reformer was modeled by implementing a settable conversion of CO_2, in accordance with Eq. 18. A unit displaying the rWGS chemical equilibrium at the chosen process conditions was implemented after the steam reformer. The CO_2 conversion was set corresponding to the chemical equilibrium.

Further information concerning steam reforming catalysts is provided by de Klerk, Lopez et al. and Schädel et al. [13,60,61].

2.7. Heat balancing

Table 3 displays the PtL plant's heat sources and sinks at their respective temperature levels. Heat balances for all analyzed process configurations have been created. A way to meet the plant's heat demand is to increase the mass flow rate of burned tail gas. However, doing so concludes in smaller shares of recirculated tail gas and, thus, declines in the PtL plant's KPIs, e.g., Power-to-Liquid efficiency and Fischer-Tropsch product streams.

The following assumptions have been made concerning the respective CO_2 sources:

1. Cement plant as CO_2 source:
   The cement plant's waste heat covers a third of the MEA absorption heat demand [29,5]. In addition, the heat demand for the provision of stripping steam is internally covered by the Fischer-Tropsch reaction heat. Thus, the remaining specific heat demand of the MEA absorption process is set at 1 GJ/t CO_2. A recirculation rate of RR = 85% can be realized while covering the PtL plant's heat demand.
2. Biogas upgrading plant as CO_2 source:
   No additional CO_2 capture unit is required for this setup. A recirculation ratio of RR = 90% can be realized.
3. CHP plant burning wood chips as CO_2 source:
   Two scenarios were defined for this plant configuration. Within the first scenario, it is assumed that the CHP plant covers the MEA absorption's heat demand, and thus, a recirculation ratio of RR = 90% is realized. Additional tail gas is combusted in the second scenario to meet the PtL plant's heat demand resulting in a recirculation ratio of only RR = 75%.

3. Results

The following chapter includes the designed flowcharts of the simulated Power-to-Liquid plant as well as the results of the three analyzed process configurations based on the following CO_2 sources.

1. Norcem Brevik cement plant in Porsgrunn, Norway [7].

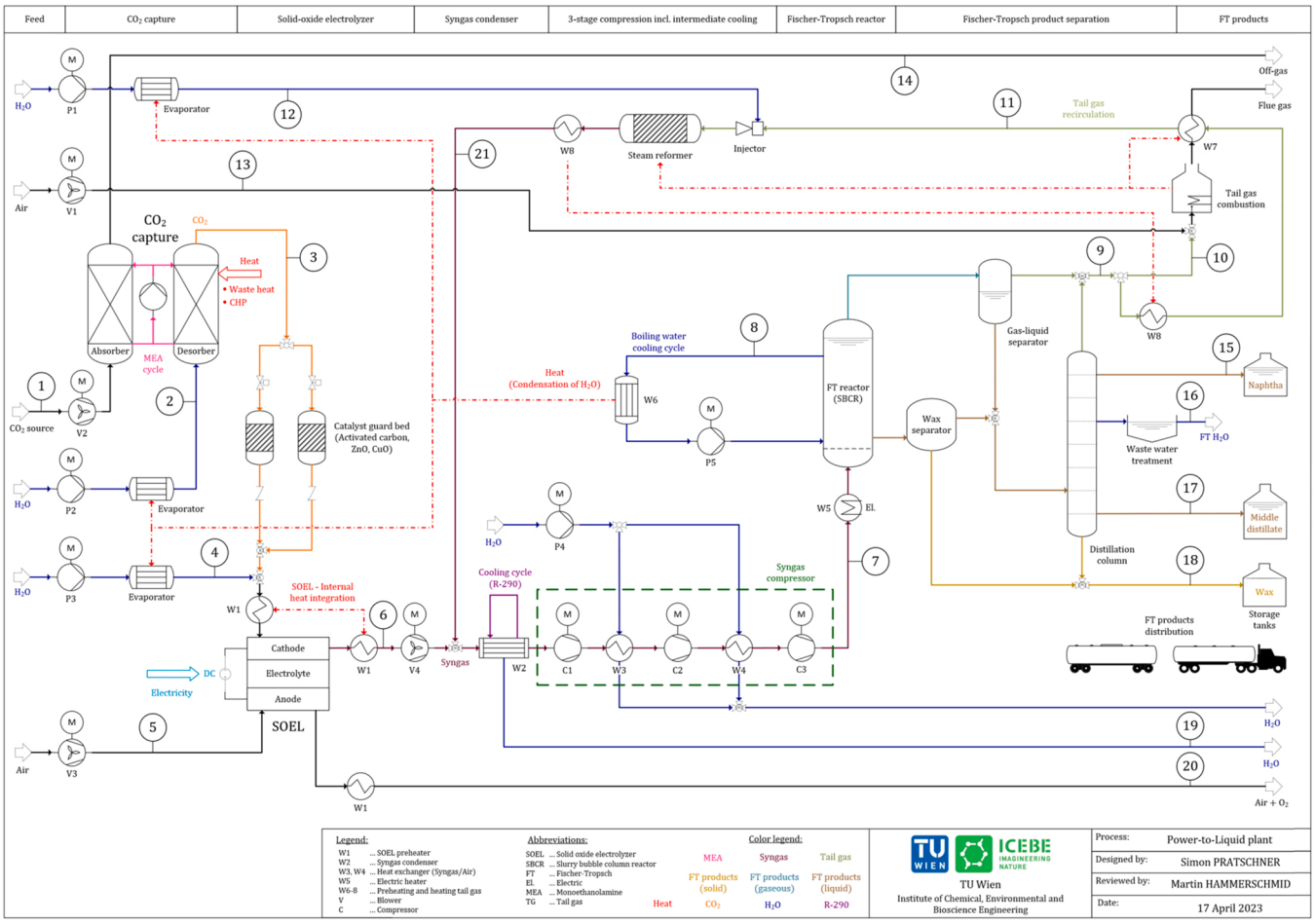

Fig. 3. Process flow diagram of a Power-to-Liquid plant based on high-temperature electrolysis and Fischer-Tropsch synthesis. The streams' mass flow rates for the respective CO_2 sources are listed in Table A.1 in the appendix.

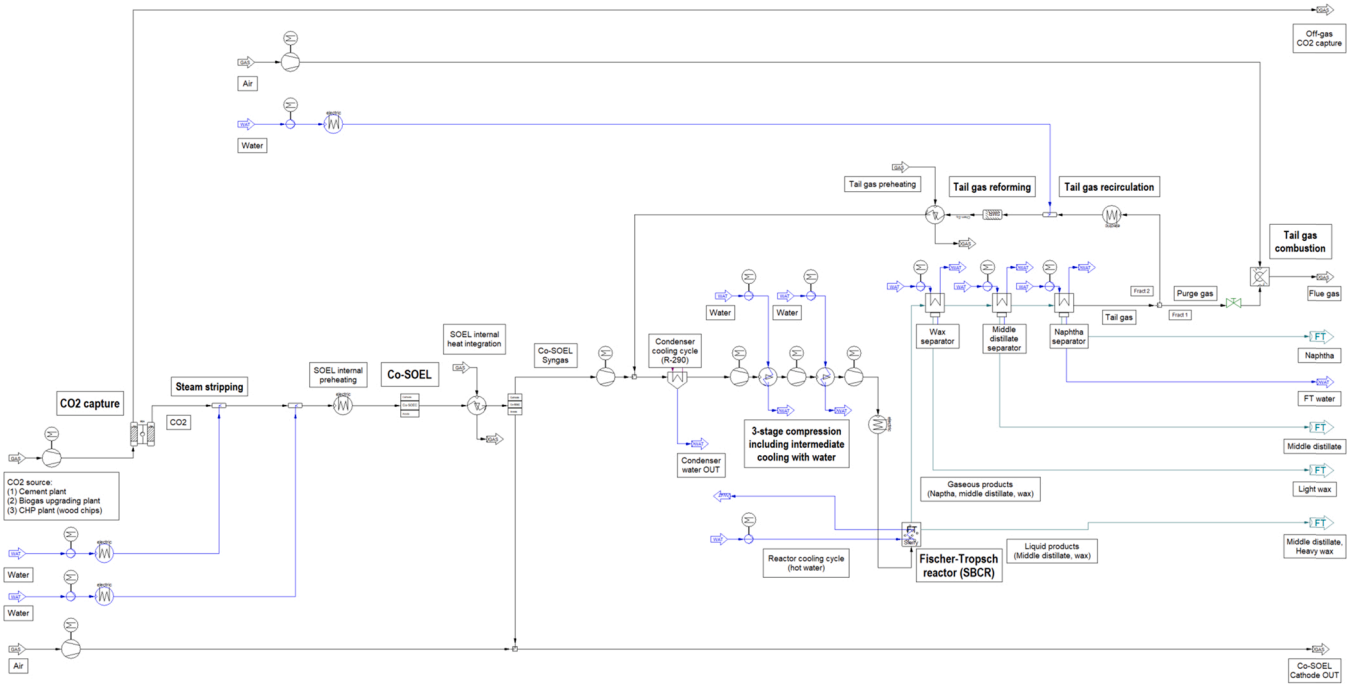

Fig. 4. Implementation of the designed Power-to-Liquid plant as process simulation flowchart in IPSEpro.

Table 4
Key performance indicators of scenario (1) - cement plant as a CO_2 source.

Key performance indicator	Symbol	Value	Unit
Carbon efficiency	η_{Carbon}	75.7	%
Power-to-Liquid efficiency	η_{PtL}	58.8	%
CO conversion	X_{CO}	93.3	%
Recirculation ratio	RR	85.0	%
SOEL scale	P_{SOEL}	504.0	$MW_{el.}$

Table 5
Input and output streams of scenario (1) - cement plant as a CO_2 source.

Input streams	Description	[t/h]	Output streams	Description	[t/h]
Flue gas	Cement plant	404.6	Naphtha	FT products	6.4
CO_2	Utilized CO_2	100.0	Middle distillate	FT products	10.1
H_2O_{MEA}	Stripping of CO_2	53.2	Wax	FT products	10.6
H_2O_{SOEL}	Additional feed	45.6	H_2O_{FT}	Waste water	37.3
$H_2O_{Reformer}$	Steam reformer	3.1	H_2O	Condenser	18.1
Ambient air	Anode purging	96.6	Flue gas	TG combustion	156.0
Ambient air	TG combustion	143.5	Off-gas_{MEA}	Desorber out	304.6
			O_2 enriched air	Anode out	203.4

Table 6
Power demand of scenario (1) - cement plant as a CO_2 source.

Process	Power demand [$MW_{el.}$]	Relative demand [%]
SOEL	504.0	89.1
Syngas compression	40.2	7.1
Syngas condenser	4.8	0.8
CO_2 capture	11.1	2.0
Auxiliaries	5.4	1.0
SUM	565.5	100.0

Table 7
Heat balance of scenario (1) - cement plant as a CO_2 source.

Heat sources			Heat sinks		
Unit	Material	Heat [$MW_{th.}$]	Unit	Material	Heat [$MW_{th.}$]
TG comb.	Flue gas	54.5	CO_2 capt.[1)]	MEA sol.	28.0
FT react.	Steam	91.8	CO_2 capt.	H_2O	38.8
W8	Tail gas	36.5	SOEL	H_2O feed	35.0
W1	Syngas	69.0	Reformer	H_2O feed	0.5
			SOEL ΔH_r	-	22.0
			Reformer ΔH_r	-	7.5
			W7	Tail gas	39.0
			SOEL	CO_2 and H_2O	66.0
SUM	-	251.8	SUM	-	236.8

1) 33% of the CO_2 capture unit's heat demand is covered by the cement plant's waste heat.

2. Biogas upgrading plant in Montello, Italy [15].
3. Decentralized CHP plant burning wood chips [56].

Based on the CO_2 sources mentioned above, the evaluated process routes will be assessed concerning their respective KPIs, as defined in chapter 2.2, and their mass and energy balances.

3.1. Process flow diagram and process simulation flowchart

Fig. 3 shows a process flow diagram of the designed Power-to-Liquid plant. The corresponding mass flow rates for the evaluated CO_2 sources are listed in table A.1 in the appendix. The processed gas stream provided by the respective CO_2 source is slightly pressurized to overcome the MEA absorption's pressure drop. After being cleaned by a catalyst guard bed, the pure CO_2 stream is mixed with steam and inserted into the SOEL unit. The generated syngas is then transferred to a condenser to avoid water condensation in the downstream syngas compressor. Subsequently, the syngas is pressurized and fed into the Fischer-Tropsch reactor. A heater at the reactor's inlet, W5, is required for plant start-up. However, this heater is inactive once steady-state operation has been reached. The streams, drained from the Fischer-Tropsch reactor, i.e., liquid and gaseous, are further processed and separated into the respective product fractions. Unconverted syngas and non-condensable hydrocarbons, i.e., methane, ethane and propane, are either recirculated and transferred to the tail gas reformer or the tail gas combustor. The recirculated tail gas share is heated and processed by a steam reformer before being mixed with the fresh syngas generated by the SOEL unit. The implementation of the designed process in IPSEpro is depicted in Fig. 4.

3.2. Cement plant as CO_2 source of the designed Power-to-Liquid plant

The first process configuration is based on a cement plant as a CO_2 source. Further details concerning the cement plant's off-gas properties are given in chapter 2.1.

3.2.1. Key performance indicators of scenario (1) – cement plant

The determined KPIs of a Power-to-Liquid plant utilizing CO_2 generated by a cement plant are listed in Table 4. With the presented concept, a carbon efficiency of 75.7% and a Power-to-Liquid efficiency of 58.8% are obtained. Varying the specific power demand of the SOEL unit from 3.2 to 3.7 kWh/Nm^3 H_2 results in a Power-to-Liquid efficiency ranging from 54.1% to 61.6%. A share of 15% of the generated tail gas must be combusted to meet the PtL plant's heat demand, concluding in a total CO conversion of 93.3%. The electrolyzer's scale is slightly above 500 $MW_{el.}$ power input to process a mass flow rate of 100 t/h CO_2.

3.2.2. Mass balance and gas compositions of scenario (1) – cement plant

Significant mass flow rates of this process route are listed in table A.1 in the appendix. The respective process stream numbers are defined in Fig. 3. A summary of all input and output streams is listed in Table 5. A mass flow rate of 100 t/h CO_2 is converted to 27.1 t/h Fischer-Tropsch products. A total water demand of 101.9 t/h is necessary to supply the CO_2 capture unit, the electrolyzer and the tail gas reformer. In addition, a mass flow rate of 240.1 t/h air is required to purge the electrolyzer's anodic layer of O_2 and to ensure a complete tail gas combustion. Relevant compositions of gas streams within the PtL plant are stated in table A.2 in the appendix. The H_2:CO ratio provided by the electrolyzer needs to be at 2.46 to ensure an H_2:CO ratio of 2.0 at the Fischer-Tropsch reactor's inlet.

3.2.3. Power and heat balances of scenario (1) – cement plant

The plant's power balance is listed in Table 6. The electrolyzer is the primary power consumer, being responsible for a relative share of almost 90%. Additionally, syngas compression accounts for around 7% of the plant's power demand. Additional power consumption for fluid conveying, caused by blowers and pumps, is almost negligible, with only 1%. The heat balance of process configuration (1) can be found in Table 7. Further details concerning the respective temperature levels are stated in Table 3, see chapter 2.7.

Table 8
Key performance indicators of scenario (2) - biogas upgrading plant as a CO_2 source.

Key performance indicator	Symbol	Value	Unit
Carbon efficiency	η_{Carbon}	88.6	%
Power-to-Liquid efficiency	η_{PtL}	63.8	%
CO conversion	X_{CO}	95.5	%
Recirculation ratio	RR	90.0	%
SOEL scale	P_{SOEL}	23.1	$MW_{el.}$

Table 9
Input and output streams of scenario (2) - biogas upgrading plant as a CO_2 source.

Input streams	Description	[t/h]	Output streams	Description	[t/h]
CO_2 rich off-gas	Biogas plant	4.6	Naphtha	FT products	0.3
CO_2	Utilized CO_2	4.5	Middle distillate	FT products	0.5
H_2O_{SOEL}	H_2O feed SOEL	4.5	Wax	FT products	0.5
$H_2O_{Reformer}$	Steam reformer	0.2	H_2O_{FT}	Waste water	1.8
Ambient air	Anode purging	4.4	H_2O	Condenser	0.9
Ambient air	TG combustion	4.8	Flue gas	TG combustion	5.2
			O_2 enriched air	Anode out	9.3

Table 10
Power demand of scenario (2) - biogas upgrading plant as a CO_2 source.

Process	Power demand [$MW_{el.}$]	Relative demand [%]
SOEL	23.1	90.9
Syngas compression	1.9	7.5
Syngas condenser	0.2	0.8
Auxiliaries	0.2	0.8
SUM	25.4	100.0

Table 11
Heat balance of scenario (2) - biogas upgrading plant as a CO_2 source.

Heat sources			Heat sinks		
Unit	Material	Heat [$MW_{th.}$]	Unit	Material	Heat [$MW_{th.}$]
TG comb.	Flue gas	1.8	SOEL	H_2O feed	3.3
FT react.	Steam	4.5	Reformer	H_2O feed	0.04
W8	Tail gas	1.9	SOEL ΔH_r	-	1.0
W1	Syngas	3.2	Reformer ΔH_r	-	0.5
			W7	Tail gas	2.1
			SOEL	CO_2 and H_2O	3.1
SUM	-	11.4	SUM	-	10.04

3.3. Biogas upgrading plant as CO_2 source of the designed Power-to-Liquid plant

The second scenario processes a CO_2-rich off-gas stream emitted by a biogas upgrading plant. The underlying assumptions regarding the CO_2 stream's properties are listed in chapter 2.1, see Table 2.

3.3.1. Key performance indicators of scenario (2) – biogas upgrading plant

The obtained KPIs of a PtL plant utilizing CO_2 of a biogas upgrading plant are listed in Table 8. Due to the CO_2 stream's high purity of 98 vol %, additional processing by an MEA absorption cycle is not required. Hence, a high tail gas recirculation ratio of 90% can be implemented, leading to a high carbon efficiency of 88.6% and an excellent Power-to-Liquid efficiency of 63.8%. A medium-scale electrolyzer with a power input of 23.1 $MW_{el.}$ is required to process the given mass flow rate of 4.5 t/h CO_2.

Table 12
Key performance indicators of scenarios (3.1) and (3.2) - utilization of CO_2 emitted by a biomass heating plant.

Key performance indicator	Scenario Symbol	(3.1)[1] Value	(3.2)[2]	Unit
Carbon efficiency	η_{Carbon}	80.0	68.4	%
Power-to-Liquid efficiency	η_{PtL}	60.9	54.7	%
CO conversion	X_{CO}	95.5	88.8	%
Recirculation ratio	RR	90.0	75.0	%
SOEL scale	P_{SOEL}	39.4	37.8	$MW_{el.}$

1) RR = 90% - the CO_2 capture unit's heat demand is covered by the CHP process
2) RR = 75% - the CO_2 capture unit's heat demand is covered by an increased share of combusted tail gas.

3.3.2. Mass balance and gas compositions of scenario (2) – biogas upgrading plant

Table 9 summarizes the input and output streams of a Power-to-Liquid plant valorizing the off-gas stream of a biogas upgrading plant. A more detailed mass balance is listed in table A.1 in the appendix. A stream of 4.5 t/h CO_2 is processed to 1.3 t/h Fischer-Tropsch products. Compared to process configurations (1) and (3), no additional purification of the feed stream by an MEA absorption unit is required. Due to this configuration's missing CO_2 stripping unit, the electrolyzer's whole H_2O demand must be injected after the catalyst guard bed. Detailed information regarding the gas composition of syngas, tail gas and the anode's purge gas stream is listed in table A.2 in the appendix.

3.3.3. Power and heat balances of scenario (2) – biogas upgrading plant

Converting CO_2 and H_2O to syngas accounts for almost 91% of the total power demand for a process configuration based on a biogas upgrading plant as a CO_2 source, as listed in Table 10. Similar to process route (1), the power demand of the syngas condenser and auxiliaries can be neglected. The syngas compressor consumes 7.5% of the Power-to-Liquid plant's electricity demand. The relatively small scale of biogas upgrading plants concludes in a medium-scale Power-to-Liquid plant with a total power consumption of 25.4 $MW_{el.}$. A detailed list of the heat sources and sinks is given in Table 11. Since no additional CO_2 capture unit is required, only 10% of the tail gas must be combusted to meet the PtL plant's heat demand.

3.4. CHP plant burning wood chips as CO_2 source of the designed Power-to-Liquid plant

The last of the three analyzed process routes is a bioenergy with carbon capture and utilization (BECCU) scenario based on CO_2 emitted by a CHP plant burning wood chips. Within the presented route, two scenarios have been analyzed:

1. In the first scenario, the remaining heat demand of the CO_2 capture unit is covered by the CHP process. Thus, the combustor's performance is decreased, and less heat can be utilized. A share of 90% of recirculated tail gas can be realized in scenario (3.1).
2. The CHP process's power and heat generation remain untouched in the second scenario. Hence, a larger share of tail gas must be combusted to ensure a sufficient heat supply for the CO_2 capture unit. Within scenario (3.2), only 75% of the tail gas can be recirculated.

Detailed information concerning the CHP process's assumptions and

Table 13
Input and output streams of scenarios (3.1) and (3.2) – utilization of CO_2 emitted by a biomass heating plant.

Input streams	Scenario Description	(3.1)[1] Mass flow rate [t/h]	(3.2)[2]	Output streams	Scenario Description	(3.1) Mass flow rate [t/h]	(3.2)
Flue gas	CHP plant	41.2	41.2	Naphtha	FT products	0.5	0.5
CO_2	Utilized CO_2	7.7	7.7	Middle dist.	FT products	0.8	0.7
H_2O_{MEA}	Stripping of CO_2	4.1	4.1	Wax	FT products	0.9	0.7
H_2O_{SOEL}	Additional feed	3.6	3.2	H_2O_{FT}	Waste water	3.0	2.6
$H_2O_{Reformer}$	Steam reformer	0.3	0.2	H_2O	Condenser	1.5	1.3
Ambient air	Anode purging	7.5	7.2	Flue gas	TG combustion	8.4	18.0
Ambient air	TG combustion	7.8	16.5	Off-gas_{MEA}	Desorber out	33.5	33.5
				O_2 enriched air	Anode out	15.9	15.3

1) RR = 90% - the CO_2 capture unit's heat demand is covered by the CHP process
2) RR = 75% - the CO_2 capture unit's heat demand is covered by an increased share of combusted tail gas.

Table 14
Power demand of scenarios (3.1) and (3.2) - utilization of CO_2 emitted by a biomass heating plant.

Scenario Process	(3.1)[1] Power demand [$MW_{el.}$]	(3.2)[2]	(3.1)[1] Relative demand [%]	(3.2)[2]
SOEL	39.4	37.8	88.7	89.4
Syngas compression	3.3	2.8	7.4	6.6
Syngas condenser	0.4	0.4	0.9	0.9
CO_2 capture	0.9	0.9	2.0	2.1
Auxiliaries	0.4	0.4	0.9	0.9
SUM	44.4	42.3	100	100

1) RR = 90% - the CO_2 capture unit's heat demand is covered by the CHP process
2) RR = 75% - the CO_2 capture unit's heat demand is covered by an increased share of combusted tail gas.

performance can be found in [56].

3.4.1. Key performance indicators – CHP plant combusting wood chips as CO_2 source (BECCU)

The KPIs of scenario (3) can be found in Table 12. Within scenario (3.1), the CO_2 capture unit's remaining heat demand is covered by the CHP process, and thus, 90% of the tail gas can be recirculated. Exploiting a fraction of the CHP process heat results in elevated KPIs of the subsequent PtL plant. A carbon efficiency of 80.0% and a PtL efficiency of 60.9% are realized. The electrolyzer's scale is 39.4 $MW_{el.}$, processing an input stream of 7.7 t/h CO_2. For scenario (3.2), the PtL plant's KPIs diminish, with a carbon efficiency of only 68.4% and a PtL efficiency of 54.7%. Additionally, the SOEL unit's scale is slightly reduced to a rated power of 37.8 $MW_{el.}$.

3.4.2. Mass balance and gas compositions – CHP plant combusting wood chips as CO_2 source

The input and output streams of scenario (3) are summarized in Table 13. A mass flow rate of 7.7 t/h CO_2 needs to be processed by the PtL plant. Mass flow rates of 7.5–8.0 t/h H_2O are required to produce a total mass flow rate of 1.9–2.2 t/h Fischer-Tropsch products. In addition, around 3.0 t/h of Fischer-Tropsch waste water needs to be treated. Detailed mass balances, including feed and product streams, are given in table A.1 in the appendix.

The differences in the respective gas compositions of scenario (3.1)

Table 15
Heat balance of scenarios (3.1) and (3.2) - utilization of CO_2 emitted by a biomass heating plant.

Heat sources Scenario Unit	Material	(3.1)[1, 2] Heat [$MW_{th.}$]	(3.2)[3]	Heat sinks Scenario Unit	Material	(3.1) Heat [$MW_{th.}$]	(3.2)
TG combustor	Flue gas	2.9	6.3	CO_2 capture	MEA solution	4.7	4.7
FT reactor	Steam	7.5	6.4	CO_2 capture	H_2O stripping	3.0	3.0
W8	Tail gas	3.1	2.2	SOEL	H_2O feed	2.6	2.4
W1	Syngas	5.4	5.2	Reformer	H_2O feed	0.04	0.04
				SOEL ΔH_r	-	1.7	1.7
				Reformer ΔH_r	-	0.7	0.5
				W7	Tail gas	3.4	2.4
				SOEL	CO_2 and H_2O	5.1	4.9
SUM	-	18.9	20.1	SUM	-	20.9	19.6

1) A share of 10% of tail gas is combusted.
2) The MEA absorption unit's heat demand is covered by the CHP process.
3) A share of 25% of tail gas is combusted.

Table 16
Power-to-Liquid efficiency – comparison to previous studies.

Source	[3]	[11]	[63]	[57]	[77]	[53]	[28]	[22]	[43]	This study
PtL efficiency [%] – lower limit	51.0	57.0	38.0[1]	50.8[3]	57.5	46.0	41.5[5]	53.6	44.0[6]	54.7
PtL efficiency [%] – upper limit			63.0[2]	62.7[4]		67.0	51.3[5]		53.9[7]	63.8

1) Direct air capture in combination with a low-temperature electrolyzer.
2) Biogas upgrading plant in combination with a high-temperature electrolyzer.
3) Without a tail gas reformer.
4) With an idealized tail gas reformer.
5) Proton exchange membrane electrolyzer vs. solid-oxide electrolyzer.
6) Proton exchange membrane electrolyzer in combination with an e-rWGS reactor.
7) High-temperature electrolysis.

Table 17
Key performance indicators of the Power-to-Liquid plant for the respective CO_2 sources.

	CO_2 source		Cement	Biogas upgrading	Solid biomass CHP	
Key performance indicator	Symbol	Unit	(1)	(2)	(3.1)[1)]	(3.2)[2)]
Carbon efficiency	η_{Carbon}	%	75.7	88.6	80.0	68.4
Power-to-Liquid efficiency	η_{PtL}	%	58.8	63.8	60.9	54.7
CO conversion	X_{CO}	%	93.3	95.5	95.5	88.8
Recirculation ratio	RR	%	85.0	90.0	90.0	75.0
Solid-oxide electrolyzer scale	P_{SOEL}	$MW_{el.}$	504.0	23.1	39.4	37.8
CO_2 input	m_{CO_2}	t/h	100.0	4.5	7.7	7.7
Fischer-Tropsch products	m_{FT}	t/h	27.1	1.3	2.2	1.9

1) 90% tail gas recirculation - the CO_2 capture unit's heat demand is covered by the CHP process.
2) 75% tail gas recirculation - the CO_2 capture unit's heat demand is covered by tail gas combustion.

Table A.1
Mass balances of the respective CO_2 sources – all streams in t/h.

		Cement	Biogas upgrading	Solid biomass CHP	
Stream [t/h]	Number	(1)	(2)[1)]	(3.1)[2)]	(3.2)[3)]
Flue gas feed	1	400.9	-	41.2	41.2
H_2O feed desorber	2	53.2	-	4.1	4.1
CO_2 feed SOEL	3	100.0	4.5	7.7	7.7
H_2O feed SOEL	4	45.6	4.5	3.6	3.2
Air feed SOEL	5	96.6	4.4	7.5	7.2
Syngas SOEL out	6	92.0	4.2	7.1	7.0
Syngas feed FT reactor	7	147.8	7.2	12.0	10.3
H_2O cooling cycle	8	171.9	8.4	14.0	11.9
Tail gas	9	83.4	4.1	6.8	5.8
Purge gas	10	12.5	0.4	0.7	1.4
Recirculated tail gas	11	70.8	3.7	6.1	4.4
H_2O feed reformer	12	3.1	0.2	0.3	0.2
Air feed combustor	13	143.5	4.4	7.8	16.5
Off-gas MEA out	14	300.9	-	33.5	33.5
Naphtha	15	6.4	0.3	0.5	0.5
Fischer-Tropsch H_2O	16	37.3	1.8	3.0	2.6
Middle distillate	17	10.1	0.5	0.8	0.7
Wax	18	10.6	0.5	0.9	0.7
H_2O condenser out	19	18.1	0.9	1.5	1.3
O_2 enriched air	20	203.4	9.3	15.9	15.3
Reformed tail gas	21	73.9	3.9	6.4	4.6

1) MEA CO_2 capture unit is not required.
2) 90% tail gas recirculation - the CO_2 capture unit's heat demand is covered by the CHP process.
3) 75% tail gas recirculation.

and scenario (3.2) are negligible. Thus, only the obtained gas compositions of scenario (3.1) are listed in table A.2 in the appendix. An H_2:CO ratio of 2.51 needs to be provided by the SOEL unit to balance the low H_2:CO ratio of 1.50 at the tail gas reformer's outlet.

3.4.3. Power and heat balance – CHP plant combusting wood chips as CO_2 source

The power demand of both scenarios utilizing CO_2 generated by the combustion of wood chips is listed in Table 14. Increasing the share of recirculated tail gas leads to a slight increase in the SOEL unit's power demand. In addition, more power must be provided to compress the increased syngas stream. Results concerning the MEA absorption unit's power demand remain constant since the same flue gas stream is processed.

The respective heat balances of scenarios (3.1) and (3.2) are listed in Table 15. Scenario (3.1)'s heat balance is negative since the CO_2 capture's heat demand is assumed to be covered by the CHP process.

4. Discussion

Cement plants are an abundant CO_2 source responsible for 3% of the EU27's and 7% of the global CO_2 emissions. Substantial advantages of cement plants are their immense availability, the significant mass flow rates of emitted CO_2 and the fact that about 30% of the CO_2 capture unit's heat demand can be covered by waste heat. Consequently, combining cement and PtL plants results in a satisfactory carbon efficiency of $\eta_{Carbon} = 75.7\%$ and a decent PtL efficiency of $\eta_{PtL} = 58.8\%$. However, cement plants emit a mixture of fossil and inorganic CO_2 and extremely large electrolyzers, around 500 $MW_{el.}$ rated power, are required to utilize the whole off-gas stream. Thus, exploiting cement plants as CO_2 sources is not ideal for current state-of-the-art electrolyzers but will become interesting as soon as electrolyzers reach scales above 100 $MW_{el.}$. A possible approach to tackle the fossil share of CO_2 emissions is the substitution of fossil fuels with biogenic methane. In addition, CO_2 emission mitigation and avoidance could be realized by applying green H_2 as fuel in the rotary kiln of cement plants.

Around 90 PtL plants of the presented concept would be necessary to process the total EU's cement industry CO_2 emissions of 0.072 Gt CO_2 per year. Exploiting the EU27's cement industry as a CO_2 source would lead to an annual output of 19.5 million tons of FT products. An estimated share of 3% of the EU's jet fuel demand could be covered by doing so, based on the annual jet fuel consumption determined by Surgenor [69] and a Fischer-Tropsch refinery efficiency of 86% [54]. At a global scale, about 680 million tons of FT products could be produced annually based on the cement industry's CO_2 emissions. To achieve this, approximately 3000 PtL plants would be required, as presented in chapter 3.2.

Utilizing biogas upgrading plants as a CO_2 source for PtL processes has several advantages. Biogas upgrading plants provide a highly concentrated CO_2 stream, making a downstream CO_2 capture unit unnecessary. As a result, the combination of biogas upgrading and PtL plants concludes in a superior PtL efficiency of $\eta_{PtL} = 63.8\%$ and carbon efficiency of $\eta_{Carbon} = 88.6\%$. In addition, valorizing biogenic CO_2 avails the global effort to curb the climate crisis. Biogas upgrading plants are usually located at decentralized sites and designed at a medium scale, thus ensuring a beneficial synergy with PtL plants. Electrolyzers at a scale of around 20 $MW_{el.}$ will be established within the upcoming years. Hence, developing a combined biogas upgrading and PtL plant, as presented in chapter 3.3, is feasible within the following decade.

The presented process route based on a biogas upgrading plant processes a mass flow rate of 4.5 t/h CO_2. About 4500 PtL plants at the suggested scale of $P_{SOEL} = 23$ $MW_{el.}$ are necessary to process the projected CO_2 emissions of biogas plants in Europe introduced by Millinger et al. [47]. As a result, around 47 million tons of FT products could be produced annually, corresponding to 7.3% of the EU's jet fuel demand, assuming a syncrude to jet fuel refinery efficiency of 86% [54].

Exploiting solid biomass CHP plants entails a detrimental controversy. Transferred heat is a key product of the biomass heating plant but is also required to separate the generated CO_2 from the flue gas stream. A possible solution for real applications could be to valorize only a part of the generated CO_2 stream during periods with an increased demand for heat and power by nearby settlements, e.g., in winter. In this case, optimized plant operation also needs to focus on economic circumstances, e.g., electricity and district heating prices, as well as potential revenue of Fischer-Tropsch products. Two scenarios have been analyzed within this work to evaluate this contradiction. Withdrawing heat from

Table A.2
Gas compositions of all scenarios in vol% - (1) cement plant, (2) biogas upgrading plant and (3) biomass heating plant..

[vol%] Stream (No.)	(1) Off-gas$_{MEA}$ (14)	(2)	(3)	(1) Syngas$_{SOEL}$ (6)	(2)	(3)	(1) Syngas$_{FT\ reactor}$ (7)	(2)	(3)	(1) Anode$_{SOEL}$ (20)	(2)	(3)	(1) Tail gas (9)	(2)	(3)	(1) Reformer$_{out}$ (21)	**(2)**	**(3)**
Ar	0.0	-	0.0	0.0	0.0	0.0	0.0	0.0	0.0	0.5			0.0	0.0	0.0	0.0	0.0	0.0
CH_4	0.0	-	0.0	0.0	0.5	0.0	0.02	0.4	0.02	0.0			0.5	1.2	0.5	0.05	0.1	0.05
C_2H_6	0.0	-	0.0	0.0	0.0	0.0	0.01	0.0	0.01	0.0			0.4	0.4	0.4	0.02	0.02	0.02
C_3H_8	0.0	-	0.0	0.0	0.0	0.0	0.0	0.0	0.0	0.0			0.3	0.3	0.3	0.0	0.0	0.0
CO	0.0	-	0.0	24.9	24.6	24.5	31.2	31.0	31.2	0.0			29.9	29.6	29.9	34.6	33.8	34.6
CO_2	2.3	-	1.6	4.4	4.3	4.4	5.17	5.2	5.17	0.0			11.0	11.0	11.0	5.3	5.4	5.3
H_2	0.0	-	0.0	61.1	61.1	61.5	62.4	62.2	62.4	0.0			56.0	55.6	56.0	52.0	52.08	52.0
H_2O	12.1	-	0.5	9.6	9.5	9.6	1.2	1.2	1.2	0.0			1.9	1.9	1.9	8.03	8.6	8.03
N_2	73.5	-	94.5	0.0	0.0	0.0	0.0	0.0	0.0	39.0			0.0	0.0	0.0	0.0	0.0	0.0
O_2	12.1	-	3.4	0.0	0.0	0.0	0.0	0.0	0.0	60.5			0.0	0.0	0.0	0.0	0.0	0.0

the CHP process, about 20% of the thermal input into the combustor, results in a PtL efficiency of $\eta_{PtL} = 60.9\%$ and carbon efficiency of $\eta_{Carbon} = 80.0\%$. In contrast, providing the required heat via an increased share of combusted tail gas results in an inferior PtL efficiency of $\eta_{PtL} = 54.7\%$ and carbon efficiency of $\eta_{Carbon} = 68.4\%$. BECCU has significant potential concerning the containment of global warming by substituting fossil commodities with alternative products based on biogenic CO_2. Furthermore, the implementation of electrolyzers at a scale of around 40 $MW_{el.}$ is a realistic scenario for this decade. However, it has to be stated that the EU's policy concerning the combustion of solid biomass is not yet decided and remains uncertain for intrigued investors.

An annual production capacity of 246 million tons of FT products could be realized by exploiting biomass heating plants in Europe, according to a scenario posed by Millinger et al. [47]. In doing so, 38% of the EU's jet fuel demand could be covered by implementing 14,000 PtL plants with a rated power of $P_{SOEL} = 39.4\ MW_{el.}$.

Within the presented study, PtL efficiencies of 54.7–63.8% were obtained by plant scales ranging from 20 to 500 $MW_{el.}$ power input into the electrolyzer. Table 16 offers a comparison to previously conducted studies with respect to the obtained PtL efficiencies. Valorizing CO_2 sources with even lower concentrations than the three analyzed scenarios, i.e., direct air capture, would decline the Power-to-Liquid efficiency to 52.8%, assuming a specific power demand of 2.3 $MJ_{el.}/kg\ CO_2$ [32]. In addition, a specific heat demand of 7.2 $MJ_{th.}/kg\ CO_2$ would be required. Thus, a feasible operation of Power-to-Liquid plants in combination with direct air capture cannot be realized under current conditions. To the best of the authors' knowledge, deriving the CO_2 source's influence on the carbon efficiency η_{Carbon} of PtL plants has not been performed by previous studies. The underlying work determined carbon efficiencies between 68.4% for a solid biomass CHP plant and 88.6% for a biogas upgrading plant.

In contrast to past studies, the performed work focuses on the CO_2 source itself by directly analyzing the key performance indicators of Power-to-Liquid plants as a function of the CO_2 source's properties. The Power-to-Liquid efficiency has been a significant indicator in previous studies. However, carbon efficiency itself has not gained the required attention. Furthermore, the underlying work improves preceding studies conducted by the authors by implementing detailed models of the solid-oxide electrolyzer, the steam reformer and the CO_2 capture unit.

5. Conclusions

The objective of this study was to answer the following research questions.

1. Which CO_2 sources should be prioritized for carbon capture and utilization applications based on Power-to-Liquid processes combining solid-oxide electrolysis and Fischer-Tropsch synthesis?
2. Which effect does the CO_2 source have on the key performance indicators of Power-to-Liquid plants?

To reach this goal, three different CO_2 sources, i.e., a cement plant, a biogas upgrading plant and a solid biomass combined heat and power plant, were analyzed concerning their influence on the performance of a Power-to-Liquid plant. Several subprocesses, i.e., CO_2 capture, solid-oxide electrolyzer, Fischer-Tropsch synthesis and steam reforming, were modeled and simulated using IPSEpro, a stationary equation-based process simulation tool. The respective key performance indicators, summarized in Table 17, as well as mass and energy balances, were determined for the assumed CO_2 sources. The results show that a maximum Power-to-Liquid efficiency of 63.8% can be achieved by exploiting biogas upgrading plants as a CO_2 source. Likewise, the maximum carbon efficiency of 88.6% is realized by the biogas upgrading process route. Capturing CO_2 from sources with a low concentration is energy-intensive [32,39]. Hence, CO_2 sources with either high concentrations or an abundance of waste heat should be prioritized to increase the Power-to-Liquid plant's share of recirculated tail gas. The detrimental effect of lacking waste heat source leads to a significant decrease in carbon, − 11.6%, and Power-to-Liquid efficiency, − 6.2%, as can be seen by comparing scenarios (3.1) and (3.2) in Table 17. This effect is caused by a decrease in the tail gas recirculation ratio required to increase the purge gas combustion's thermal load. Very large electrolyzers with a rated power of around 500 $MW_{el.}$ are required to utilize cement plant off-gas streams entirely, whereas medium-scale electrolysis units, approximately 20–40 $MW_{el.}$, can process CO_2 streams emitted by decentralized biogas and solid biomass heating plants. The mass flow rate of Fischer-Tropsch products ranges from 1.3 t/h (biogas upgrading plant) to 27.1 t/h (cement plant). The required water mass flow rate ranges from 4.7 t/h to 101.9 t/h, respectively.

Power-to-Liquid plants have the potential to curb the climate crisis by converting CO_2, water and electricity into Fischer-Tropsch products, which can subsequently be processed into synthetic fuels for the aviation, marine and heavy-duty industry. Especially plants valorizing biogenic CO_2 should be a linchpin of the EU's transition toward an ecologically and economically sustainable energy system. In addition, Power-to-Liquid plants ensure political and economic independence by exploiting local CO_2 sources instead of fossil imports. CO_2 sources are abundant and show significant differences concerning their properties. This study provides the necessary information to choose the most effective and efficient CO_2 sources concerning the plants' realizable carbon and Power-to-Liquid efficiency. Electricity is a scarce and precious resource. Hence, maximizing the Power-to-Liquid efficiency of Power-to-Liquid plants is inevitable for conscientious and sustainable electricity utilization. Additionally, the provided mass and energy balances facilitate the decision-making process of significant CO_2 emitters, e.g., companies and communities, whether their CO_2 sources should be exploited by a downstream Power-to-Liquid plant.

The underlying process simulation is solely based on static operating points, thus, leaving room for improvement by assessing the presented plant concept with a dynamic process simulation tool. In doing so, the electrolyzer's dynamic behavior, as well as uncertainties caused by intermittent renewable power sources, could be analyzed for an

extended period of plant operation. In addition, energy storage technologies, e.g., batteries or a syngas buffer tank, could be integrated and evaluated for different scenarios. Heat balances were determined within the presented plant concept. However, further elaboration, e.g., by designing a heat exchanger network, is necessary to achieve the determined efficiencies for real applications. Additionally, downstream processing of Fischer-Tropsch products is vital to ensure national standards and requirements concerning aviation and maritime navigation fuels.

Future projects founded on the presented study could implement a more sophisticated process simulation environment by designing dynamic models for the respective subprocesses. One possible question could be whether grid-powered or stand-alone solutions, directly powered by renewable energy sources, should be prioritized to ensure an economical and sustainable operation of Power-to-Liquid plants. Designing and optimizing a power supply system consisting of renewable power sources, e.g., wind and solar, combined with a grid connection, is required to boost technical practicability. In addition, an ecologic evaluation of the presented plant concept needs to be conducted to assess the environmental impact of the process and Fischer-Tropsch products. Furthermore, a techno-economic assessment, primarily focusing on the effects of an increase in the Power-to-Liquid plant scale, is required to evaluate the cost-competitiveness of synthetic fuels based on Fischer-Tropsch products with conventional fossil fuels.

Funding

The underlying work has received funding from the Mobility of the Future program – a research, technology and innovation funding program of the Federal Ministry of Climate Action, Environment, Energy, Mobility, Innovation and Technology, Republic of Austria. The Austrian Research Promotion Agency (FFG) has been authorized for the program management of the project “IFE – Innovation Flüssige Energie” (project #884340). In addition, the authors would like to thank TU Wien Bibliothek for covering article processing charges through its Open Access Funding program.

CRediT authorship contribution statement

Conceptualization: **Simon Pratschner, Martin Hammerschmid, Stefan Müller, Franz Winter:** Methodology: **Simon Pratschner, Martin Hammerschmid:** Software: **Simon Pratschner, Martin Hammerschmid, Stefan Müller:** Validation: **Simon Pratschner, Martin Hammerschmid:** Formal analysis: **Simon Pratschner:** Investigation: **Simon Pratschner:** Resources: **Stefan Müller, Franz Winter:** Data curation: **Martin Hammerschmid:** Writing – Original draft: **Simon Pratschner:** Writing – Review and editing: **Simon Pratschner, Martin Hammerschmid, Stefan Müller, Franz Winter:** Visualization: **Simon Pratschner:** Supervision: **Stefan Müller, Franz Winter:** Project administration: **Martin Hammerschmid, Stefan Müller, Franz Winter:** Funding acquisition: **Stefan Müller, Franz Winter**.

Declaration of Competing Interest

The authors declare that they have no known competing financial interests or personal relationships that could have appeared to influence the work reported in this paper.

Data availability

Data will be made available on request.

Acknowledgements

The authors would like to acknowledge the “IFE – Innovation Flüssige Energie” project consortium, the TU Wien doctoral college CO_2Refinery and the open access funding by TU Wien.

Appendix

.

References

[1] S.G. Adiya, Z.I. Dupont, V. Mahmud, T, Chemical equilibrium analysis of hydrogen production from shale gas using sorption enhanced chemical looping steam reforming, Fuel Process. Technol. 159 (2017) 128–144, https://doi.org/10.1016/j.fuproc.2017.01.026.

[2] S. Ali, K. Sørensen, M.P. Nielsen, Modeling a novel combined solid oxide electrolysis cell (SOEC) - biomass gasification renewable methanol production system, Renew. Energy 154 (2020) 1025–1034, https://doi.org/10.1016/j.renene.2019.12.108.

[3] W.L. Becker, R.J. Braun, M. Penev, M. Melaina, Production of Fischer–Tropsch liquid fuels from high temperature solid oxide co-electrolysis units, Energy 47 (2012) 99–115, https://doi.org/10.1016/j.energy.2012.08.047.

[4] G. Bianchi, G.P. Panayiotou, L. Aresti, S.A. Kalogirou, G.A. Florides, K. Tsamos, S. A. Tassou, P. Christodoulides, Estimating the waste heat recovery in the European Union Industry, Energ. Ecol. Environ. 4 (2019) 211–221, https://doi.org/10.1007/s40974-019-00132-7.

[5] L.-M. Bjerge, P. Brevik, CO_2 capture in the cement industry, norcem CO_2 capture project (Norway), Energy Procedia 63 (2014) 6455–6463, https://doi.org/10.1016/j.egypro.2014.11.680.

[6] A. Bosoaga, O. Masek, J.E. Oakey, CO_2 capture technologies for cement industry, Energy Procedia 1 (2009) 133–140, https://doi.org/10.1016/j.egypro.2009.01.020.

[7] Brevik C.C.S. 2022, Brevik CCS – World’s first CO2 capture facility at a cement plant. Available at: https://www.brevikccs.com/en. (Accessed: 22.12.2022).

[8] Buysse. C. and Miller. J. The International Council on Clean Transportation, 2021. Transport could burn up the EU’s entire Carbon Budget. Available at: https://theicct.org/transport-could-burn-up-the-eus-entire-carbon-budget/#:~:text=Yet%2C%20even%20under%20the%20most,than%20the%20entire%20EU%20economy’s. (Accessed: 27.12.2022).

[9] G. Caposciutti, A. Baccioli, L. Ferrari, U. Desideri, Biogas from anaerobic digestion: power generation or biomethane production? Energies 13 (2020) 743, https://doi.org/10.3390/en13030743.

[10] C. Carbone, D. Ferrario, A. Lanzini, S. Stendardo, A. Agostini, Evaluating the carbon footprint of cement plants integrated with the calcium looping CO_2 capture process, Front. Sustain 3 (2022), 809231, https://doi.org/10.3389/frsus.2022.809231.

[11] G. Cinti, G. Discepoli, G. Bidini, A. Lanzini, M. Santarelli, Co-electrolysis of water and CO $_2$ in a solid oxide electrolyzer (SOE) stack: Study of high-temperature co-electrolysis reactions in SOEC, Int. J. Energy Res. 40 (2016) 207–215, https://doi.org/10.1002/er.3450.

[12] Giovanni Cinti, A. Baldinelli, A. Di Michele, U. Desideri, Integration of solid oxide electrolyzer and Fischer-Tropsch: a sustainable pathway for synthetic fuel, Appl. Energy 162 (2016) 308–320, https://doi.org/10.1016/j.apenergy.2015.10.053.

[13] A. de Klerk, Fischer-Tropsch Refining, 1st. ed., Wiley-VCH,, Weinheim, Germany, 2011.

[14] Emele, L., Graichen, J., Mendelevitch, R., 2021, Decomposition analysis of CO2 emissions in the European cement sector. German Environment Agency, Berlin, Germany.

[15] E. Esposito, L. Dellamuzia, U. Moretti, A. Fuoco, L. Giorno, J.C. Jansen, Simultaneous production of biomethane and food grade CO $_2$ from biogas: an industrial case study, Energy Environ. Sci. 12 (2019) 281–289, https://doi.org/10.1039/C8EE02897D.

[16] European Environment Agency. 2022. Greenhouse gas emissions from transport in Europe. Available at: https://www.eea.europa.eu/ims/greenhouse-gas-emissions-from-transport. (Accessed: 21.12.2022).

[17] European Environment Agency. 2022a. Primary and final energy consumption in Europe. Available at: https://www.eea.europa.eu/ims/primary-and-final-energy-consumption#:~:text=The%2032.5%20%25%20target%20for%202030,the%20EU%2D27%20in%202030. (Accessed: 22.12.2022).

[18] European Parliament. 2022. Emissions from planes and ships: facts and figures. Available at: https://www.europarl.europa.eu/news/en/headlines/society/20191129STO67756/emissions-from-planes-and-ships-facts-and-figures-infographic. (Accessed: 21.12.2022).

[19] R. Feiz, M. Johansson, E. Lindkvist, J. Moestedt, S.N. Påledal, F. Ometto, The biogas yield, climate impact, energy balance, nutrient recovery, and resource cost of biogas production from household food waste—a comparison of multiple cases from Sweden, J. Clean. Prod. 378 (2022), 134536, https://doi.org/10.1016/j.jclepro.2022.134536.

[20] D. Förtsch, K. Pabst, E. Groß-Hardt, The product distribution in Fischer–Tropsch synthesis: an extension of the ASF model to describe common deviations, Chem. Eng. Sci. 138 (2015) 333–346, https://doi.org/10.1016/j.ces.2015.07.005.

[21] FuelCell Energy. 2023. Solid Oxide Electrolyzer specification sheet. Available at: https://go.fuelcellenergy.com/hubfs/solid-oxide-electrolyzer-spec-sheet.pdf. (Accessed: 14.4.2023).

[22] R. Gao, C. Zhang, K.-W. Jun, S.K. Kim, H.-G. Park, T. Zhao, L. Wang, H. Wan, G. Guan, Green liquid fuel and synthetic natural gas production via CO_2 hydrogenation combined with reverse water-gas-shift and Co-based Fischer-Tropsch synthesis, J. CO_2 Util. 51 (2021), 101619, https://doi.org/10.1016/j.jcou.2021.101619.

[23] J. Gaspar, A. Gladis, J.B. Jørgensen, K. Thomsen, N. von Solms, P.L. Fosbøl, Dynamic operation and simulation of post-combustion CO_2 capture, Energy Procedia 86 (2016) 205–214, https://doi.org/10.1016/j.egypro.2016.01.021.

[24] Handelsblatt.E-Fuels for Aviation and Marine Transportation: Federal Government funds Project in Frankfurt. Available at: https://www.handelsblatt.com/unternehmen/handel-konsumgueter/synthetische-treibstoffe-e-fuels-fuer-flugzeuge-und-schiffe-bund-foerdert-projekt-in-frankfurt/28835764.html. (Accessed: 21.12.2022).

[25] A. Hauch, K. Brodersen, M. Chen, M.B. Mogensen, Ni/YSZ electrodes structures optimized for increased electrolysis performance and durability, Solid State Ion. 293 (2016) 27–36, https://doi.org/10.1016/j.ssi.2016.06.003.

[26] HELMETH. 2018. High temperature electrolysis cell (SOEC). Available at: http://www.helmeth.eu/index.php/technologies/high-temperature-electrolysis-cell-soec. (Accessed: 23.02.2023).

[27] G. Herz, E. Reichelt, M. Jahn, Techno-economic analysis of a co-electrolysis-based synthesis process for the production of hydrocarbons, Appl. Energy 215 (2018) 309–320, https://doi.org/10.1016/j.apenergy.2018.02.007.

[28] G. Herz, C. Rix, E. Jacobasch, N. Müller, E. Reichelt, M. Jahn, A. Michaelis, Economic assessment of Power-to-Liquid processes – influence of electrolysis technology and operating conditions, Appl. Energy 292 (2021), 116655, https://doi.org/10.1016/j.apenergy.2021.116655.

[29] T. Hills, D. Leeson, N. Florin, P. Fennell, Carbon capture in the cement industry: technologies, progress, and retrofitting, Environ. Sci. Technol. 50 (2016) 368–377, https://doi.org/10.1021/acs.est.5b03508.

[30] ICO2CHEM. 2022. From industrial CO2 Streams to added value Fischer-Tropsch Chemicals. Available at: https://www.aspire2050.eu/ico2chem. (Accessed: 21.12.2022).

[31] IEA, 2021. Global Energy Review 2021. IEA - International Energy Agency, France. Available at: https://iea.blob.core.windows.net/assets/d0031107–401d-4a2f-a48b-9eed19457335/GlobalEnergyReview2021.pdf. (Accessed: 26.4.2023).

[32] IEA. 2022a. Direct Air Capture. Available at: https://www.iea.org/reports/direct-air-capture. (Accessed: 17.4.2023).

[33] IEA.2022. Cement, IEA, Paris. Available at: https://www.iea.org/reports/cement. (Accessed: 21.12.2022).

[34] Ineratec. 2022a. German e-fuel production technology to enter Japan and Asian-pacific market. Available at: https://ineratec.de/en/german-e-fuel-technology-to-enter-japan-asian-pacific-market/. (Accessed: 21.12.2022).

[35] Ineratec. 2022b. Start of Commissioning in Hamburg. Available at: https://ineratec.de/inbetriebnahmestart-in-hamburg/#:~:text=M%C3%A4rz%202022%20%E2%80%93%20In%20Hamburg%20beginnt,Chemikalien%20und%20e%2DFuels%20herstellen. (Accessed: 21.12.2022).

[36] H. Jouhara, N. Khordehgah, S. Almahmoud, B. Delpech, A. Chauhan, S.A. Tassou, Waste heat recovery technologies and applications, Therm. Sci. Eng. Prog. 6 (2018) 268–289, https://doi.org/10.1016/j.tsep.2018.04.017.

[37] Kecebas, A., Kayfeci, M., Bayat, M., 2019. Electrochemical hydrogen generation, in: Solar Hydrogen Production - Processes, Systems and Technologies.

[38] K. Kim, H. Seo, D.J. Kim, C. Lee, D.Y. Min, H.M. Kim, Y.-K. Park, Experimental evaluation of CO_2 capture with an amine impregnated sorbent in dual circulating fluidized bed process, Int. J. Greenh. Gas. Control 101 (2020), 103141, https://doi.org/10.1016/j.ijggc.2020.103141.

[39] K. Li, A. Cousins, H. Yu, P. Feron, M. Tade, W. Luo, J. Chen, Systematic study of aqueous monoethanolamine-based CO_2 capture process: model development and process improvement, Energy Sci. Eng. 4 (2016) 23–39, https://doi.org/10.1002/ese3.101.

[40] LIPOR. 2022. Cutting-edge Power-to-Liquid project transforms municipal waste-derived CO2 into sustainable aviation fuels (SAF). Available at: https://www.lipor.pt/en/press-releases/cutting-edge-power-to-liquid-project-transforms-municipal-waste-derived-co2-into-sustainable-aviation-fuels-saf/. (Accessed: 21.12.2022).

[41] H. Machida, R. Ando, T. Esaki, T. Yamaguchi, H. Horizoe, A. Kishimoto, K. Akiyama, M. Nishimura, Low temperature swing process for CO_2 absorption-desorption using phase separation CO_2 capture solvent, Int. J. Greenh. Gas. Control 75 (2018) 1–7, https://doi.org/10.1016/j.ijggc.2018.05.010.

[42] M. Marchese, E. Giglio, M. Santarelli, A. Lanzini, Energy performance of Power-to-Liquid applications integrating biogas upgrading, reverse water gas shift, solid oxide electrolysis and Fischer-Tropsch technologies, Energy Convers. Manag.: X 6 (2020), 100041, https://doi.org/10.1016/j.ecmx.2020.100041.

[43] C. Markowitsch, M. Lehner, M. Maly, Evaluation of process structures and reactor technologies of an integrated Power-to-Liquid plant at a cement factory, J. CO_2 Util. 70 (2023), 102449, https://doi.org/10.1016/j.jcou.2023.102449.

[44] Markowitsch, C., Lehner, M., Kitzweger, J., Haider, W., Ivanovici, S., Unfried, M., Maly, M., 2022. C2PAT - Carbon to Product Austria. Presented at the 17th Symposium Energieinnovation, Graz, Austria, p. 12.

[45] V. Menon, Q. Fu, V.M. Janardhanan, O. Deutschmann, A model-based understanding of solid-oxide electrolysis cells (SOECs) for syngas production by $H2O/CO_2$ co-electrolysis, J. Power Sources 274 (2015) 768–781, https://doi.org/10.1016/j.jpowsour.2014.09.158.

[46] Metz, B., Intergovernmental Panel on Climate Change (Eds.), 2005. IPCC special report on carbon dioxide capture and storage. Cambridge University Press, for the Intergovernmental Panel on Climate Change, Cambridge.

[47] M. Millinger, L. Reichenberg, F. Hedenus, G. Berndes, E. Zeyen, T. Brown, Are biofuel mandates cost-effective? – an analysis of transport fuels and biomass usage to achieve emissions targets in the European energy system, Appl. Energy 326 (2022), 120016, https://doi.org/10.1016/j.apenergy.2022.120016.

[48] R. Nassar, J.-P. Mastrogiacomo, W. Bateman-Hemphill, C. McCracken, C. G. MacDonald, T. Hill, C.W. O'Dell, M. Kiel, D. Crisp, Advances in quantifying power plant CO_2 emissions with OCO-2, Remote Sens. Environ. 264 (2021), 112579, https://doi.org/10.1016/j.rse.2021.112579.

[49] National Oceanic and Atmospheric Administration. 2022. Trends in Atmospheric Carbon Dioxide. Available at: https://gml.noaa.gov/ccgg/trends/global.html. (Accessed: 27.12.2022).

[50] Nordic Electrofuel. 2022. Plants and Projects. Available at: https://nordicelectrofuel.no/what-we-do/. (Accessed: 21.12.2022).

[51] Norsk e-fuel. 2022. Accelerating the Transition to renewable Aviation. Available at: https://www.norsk-e-fuel.com/. (Accessed: 21.12.2022).

[52] Park, K., Øi, L.E., 2017. Optimization of Gas Velocity and Pressure Drop in CO2 Absorption Column. Proceedings of the 58th SIMS. pp. 292–297. https://doi.org/10.3384/ecp17138292.

[53] R. Peters, N. Wegener, R.C. Samsun, F. Schorn, J. Riese, M. Grünewald, D. Stolten, A techno-economic assessment of Fischer–Tropsch fuels based on syngas from co-electrolysis, Processes 10 (2022) 699, https://doi.org/10.3390/pr10040699.

[54] A.M. Petersen, F. Chireshe, O. Okoro, J. Gorgens, J. Van Dyk, Evaluating refinery configurations for deriving sustainable aviation fuel from ethanol or syncrude, Fuel Process. Technol. 219 (2021), 106879, https://doi.org/10.1016/j.fuproc.2021.106879.

[55] R.C. Poudel, D. Khatiwada, P. Aryal, M. Sapkota, Large-scale biogas upgrading plants: future prospective and technical challenges, in: Emerging Technologies and Biological Systems for Biogas Upgrading, Elsevier, 2021, pp. 467–491, https://doi.org/10.1016/B978-0-12-822808-1.00017-9.

[56] S. Pratschner, P. Skopec, J. Hrdlicka, F. Winter, Power-to-green methanol via CO_2 hydrogenation—a concept study including oxyfuel fluidized bed combustion of biomass, Energies 14 (2021) 4638, https://doi.org/10.3390/en14154638.

[57] S. Pratschner, M. Hammerschmid, F.J. Müller, S. Müller, F. Winter, Simulation of a pilot scale Power-to-Liquid plant producing synthetic fuel and wax by combining Fischer–Tropsch synthesis and SOEC, Energies 15 (2022) 4134, https://doi.org/10.3390/en15114134.

[58] T. Pröll, G. Schöny, G. Sprachmann, H. Hofbauer, Introduction and evaluation of a double loop staged fluidized bed system for post-combustion CO 2 capture using solid sorbents in a continuous temperature swing adsorption process, Chem. Eng. Sci. 141 (2016) 166–174, https://doi.org/10.1016/j.ces.2015.11.005.

[59] Roy, S. and Ethakota, M., 2022. Solid oxide electrolysis cell (SOEC): Potential technology for low cost green H2. H2TECH. Available at: https://h2-tech.com/articles/2022/q4–2022/special-focus-future-of-hydrogen-energy/solid-oxide-electrolysis-cell-soec-potential-technology-for-low-cost-green-h-sub-2-sub/. (Accessed: 15.4.2023).

[60] J. Saavedra Lopez, V. Lebarbier Dagle, C.A. Deshmane, L. Kovarik, R.S. Wegeng, R. A. Dagle, Methane and ethane steam reforming over MgAl2O4-Supported Rh and Ir catalysts: catalytic implications for natural gas reforming application, Catalysts 9 (2019) 801, https://doi.org/10.3390/catal9100801.

[61] B.T. Schädel, M. Duisberg, O. Deutschmann, Steam reforming of methane, ethane, propane, butane, and natural gas over a rhodium-based catalyst, Catal. Today 142 (2009) 42–51, https://doi.org/10.1016/j.cattod.2009.01.008.

[62] O. Schmidt, A. Gambhir, I. Staffell, A. Hawkes, J. Nelson, S. Few, Future cost and performance of water electrolysis: an expert elicitation study, Int. J. Hydrog. Energy 42 (2017) 30470–30492, https://doi.org/10.1016/j.ijhydene.2017.10.045.

[63] Schmidt, P., Weindorf, W., 2016. Power-to-Liquids: Potential and Perspectives for the Future Supply of Renewable Aviation Fuel.

[64] B. Shri Prakash, S. Senthil Kumar, S.T. Aruna, Properties and development of Ni/YSZ as an anode material in solid oxide fuel cell: A review, Renew. Sustain. Energy Rev. 36 (2014) 149–179, https://doi.org/10.1016/j.rser.2014.04.043.

[65] J.S. Sravan, A. Tharak, S.V. Mohan, Status of biogas production and biogas upgrading: a global scenario, in: Emerging Technologies and Biological Systems for Biogas Upgrading, Elsevier, 2021, pp. 3–26, https://doi.org/10.1016/B978-0-12-822808-1.00002-7.

[66] C.M. Stoots, J.E. O'Brien, J.S. Herring, J.J. Hartvigsen, Syngas production via high-temperature coelectrolysis of steam and carbon dioxide, J. Fuel Cell Sci. Technol. 6 (2009), 011014, https://doi.org/10.1115/1.2971061.

[67] Sunfire. 2023. Renewable hydrogen project "Multiplhy": World's largest high-temperature electrolyzer from Sunfire successfully installed. Available at: https://www.sunfire.de/en/news/detail/renewable-hydrogen-project-multiplhy-worlds-largest-high-temperature-electrolyzer-from-sunfire-successfully-installed. (Accessed: 18.4.2023).

[68] Sunfire. 2023a. SUNFIRE-HYLINK SOEC. Available at: https://www.sunfire.de/files/sunfire/images/content/Sunfire.de%20(neu)/Sunfire-Factsheet-HyLink-SOEC-20210303.pdf. (Accessed: 18.4.2023).

[69] Surgenor, C., 2021. SAF could make up 5.5% of 2030 EU jet fuel demand with targeted support, estimates ICCT feedstock study. Available at: https://www.greenairnews.com/?p=749. (Accessed: 2.1.2023).

[70] Thyssenkrupp. 2022. The Carbon2Chem Project. Available at: https://www.thyssenkrupp.com/en/newsroom/content-page-162.html. (Accessed: 21.12.2022).

[71] S. Vaz, A.P. Rodrigues de Souza, B.E. Lobo Baeta, Technologies for carbon dioxide capture: a review applied to energy sectors, Clean. Eng. Technol. 8 (2022), 100456, https://doi.org/10.1016/j.clet.2022.100456.

[72] Yao Wang, T. Liu, L. Lei, F. Chen, High temperature solid oxide $H2O/CO_2$ co-electrolysis for syngas production, Fuel Process. Technol. 161 (2017) 248–258, https://doi.org/10.1016/j.fuproc.2016.08.009.

[73] Yuan Wang, L. Zhao, A. Otto, M. Robinius, D. Stolten, A review of post-combustion CO_2 capture technologies from coal-fired power plants, Energy Procedia 114 (2017) 650–665, https://doi.org/10.1016/j.egypro.2017.03.1209.

[74] E. Worrell, L. Price, N. Martin, C. Hendriks, L.O. Meida, Carbon dioxide emissions from the global cement industry, Annu. Rev. Energy Environ. 26 (2001) 303–329, https://doi.org/10.1146/annurev.energy.26.1.303.

[75] C. Wulf, P. Zapp, A. Schreiber, Review of Power-to-X demonstration projects in Europe, Front. Energy Res. 8 (2020) 191, https://doi.org/10.3389/fenrg.2020.00191.

[76] H. Xu, B. Chen, J. Irvine, M. Ni, Modeling of CH4-assisted SOEC for H2O/CO_2 co-electrolysis, Int. J. Hydrog. Energy 41 (2016) 21839–21849, https://doi.org/10.1016/j.ijhydene.2016.10.026.

[77] G. Zang, P. Sun, A.A. Elgowainy, A. Bafana, M. Wang, Performance and cost analysis of liquid fuel production from H2 and CO_2 based on the Fischer-Tropsch process, J. CO_2 Util. 46 (2021), 101459, https://doi.org/10.1016/j.jcou.2021.101459.